J Seismol (2012) 16:595–602
DOI 10.1007/s10950-012-9286-7

ORIGINAL ARTICLE

Rotational sensors—a comparison of different sensor types

Felix Bernauer · Joachim Wassermann · Heiner Igel

Received: 28 July 2011 / Accepted: 15 February 2012 / Published online: 2 March 2012

Abstract We present laboratory tests for two types of rotational motion sensors, the liquid-based rotational seismometers type R1 and type R2 manufactured by Eentec and the closed loop fiber optic gyroscope LCG-Demonstrator by Northrop Grumman LITEF. All instruments were calibrated absolutely at different temperatures, characterization and quantification of self-noise was carried out, and a comparison with the ring laser gyroscope G from the Geodetic Observatory in Wettzell, Germany is drawn. The generator constant of the R1 varies up to 27% in the nominal operating temperature range. In the closed-loop system LCG-Demonstrator, the compensation for temperature variation works very well, and the generator constant can be seen as constant within the error bars. For both instrument types, we measured sensitivities in the order of 10^{-7} rad/s in a period range from 10 to 100 s. While this sensitivity is already sufficient for civil engineering applications, it has to be improved by at least 1 order of magnitude for applications in weak motion seismology.

F. Bernauer (✉) · J. Wassermann · H. Igel
Department of Earth and Environmental Sciences, Ludwig-Maximilians-University, 80333 Munich, Germany
e-mail: felix.bernauer@helmholtzmuenchen.de

Keywords Rotational seismology · Instrumentation · Rotational motion sensors · Absolute calibration · Instrument self noise

1 Introduction

In the field of seismology, mainly two groups of potential applications exist in which measuring true rotational motions next to classical translational motions are proved to be very useful. In strong motion seismology, seismograms recorded by the horizontal components of a traditional pendulum accelerometer are inherently contaminated by tilt, that is, caused by a rotational ground motion around a horizontal axis (see Graizer 2006, 2010). By performing a side-by-side measurement of three transverse acceleration components and three rotation components, it is possible to correct the transverse acceleration seismograms for tilt and thus estimate the history of the true point motion (see van Driel et al., this volume).

A different approach focuses on a well-known but only recently proved relationship between rotational motion and acceleration in far field applications. Considering a transversely polarized plane wave, propagating in x-direction with displacement $\mathbf{u}(x, y, z, t) = (0, u_y(t - x/c), 0)$ and the phase velocity c, the relationship $\omega_z = -\dot{u}_y/2c$ between vertical rotation ω_z and transverse

velocity $\dot{u}_y$ is easily derived with the definition of rotation $\omega = (1/2)\nabla \times \mathbf{u}$ (Cochard et al. 2006). This proportionality has been shown experimentally by Igel et al. (2005) for the Tokachi-Oki earthquake ($M_W = 8.1$) measured by a Streckeisen STS2 seismometer and the ring laser gyroscope G operated by the Geodetic Observatory in Wettzell, Germany. A second example by Schreiber et al. (2009a) uses data from the 20 April 2006 $M7.6$ Kamchatka event recorded by a Lennartz LE3D 20-s seismometer and the ring laser gyroscope GEOsensor installed at the Piñon Flat Seismological Observatory, California.

For such applications we formulate the following a-priori requirements for rotational motion sensors for seismological applications: (1) The sensor needs to be effectively insensitive to linear motion, or at any rate, distinct measurement of linear and rotational motions must be possible. (2) For installing networks of temporary stations the instrument needs to be small and stable with respect to ambient conditions, including changes in temperature. (3) Similarly, the electrical power supply should be easily managed with batteries, at least in combination with solar panels or fuel cells. (4) A useful instrument for weak motion seismology needs to be able to measure amplitudes in the order of 10^{-7}rad/s at periods from 10 s to 100 s.

The Eentec R1 has already been used to measure rotations, for example, in the TAIGA explosion experiments by Lin et al. (2009). Tests on linear and cross-axis sensitivity for the Eentec R1 were carried out by Nigbor et al. (2009). The values they obtained (0.06 mrad/s/(m/s^2) linear sensitivity and 2% cross-axis sensitivity) are conservative maximum values. Because of its inertial mass free physical principle based on the Sagnac effect (see Schreiber et al. 2009b), the fiber optic gyroscope LCG-Demonstrator by Northrop Grumman LITEF is not sensitive to translational motions at all. The maximum value for axis misalignment given by the manufacturer is 1 mrad. This paper focuses on temperature stability of the generator constants of the R1, its succeeding model R2, and the only three existing models of the LCG-Demonstrator (S/N 2056, 2276, and 2486). Furthermore, the self-noise of all three instrument types is characterized and quantified as a function of frequency.

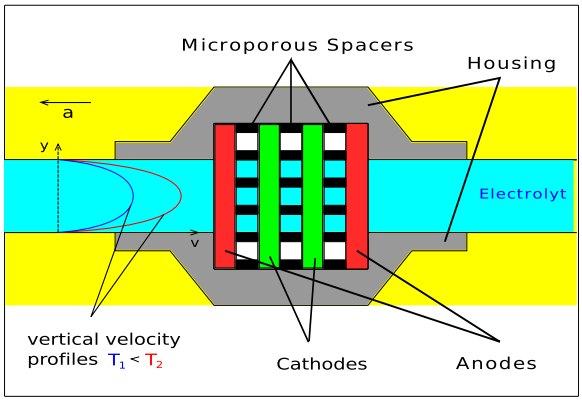

Fig. 1 The measuring device in the liquid-based rotational seismometers R1 and R2 is an electrochemical transducer consisting of two platinum mesh anodes and two platinum mesh cathodes that are sandwiched between micro-porous, isolating spacers (after Eentec 2006). The current of ions through the transducer depends on dynamic viscosity and thereby on the fluid temperature

2 Instruments

The measuring device in the liquid-based rotational seismometers R1 and R2 is an electrochemical transducer consisting of two platinum mesh anodes and two platinum mesh cathodes that are sandwiched between micro-porous, isolating spacers (Fig. 1). The electrochemical transducer and a ring-shaped tube containing an electrolyte liquid are held together by a stable housing (Eentec 2006). External rotation of the sensor and

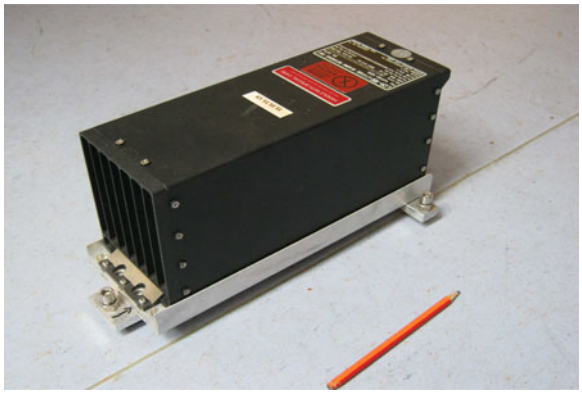

Fig. 2 The LCG-Demonstrator can measure three components of rotation with three orthogonally aligned fiber optic gyroscopes and three components of transverse acceleration using three silicon MEMS accelerometers

Table 1 Technical data provided by the manufacturers for R1, R2, and LCG-Demonstrator

	R1	R2	LCG
Frequency range	0.03 to 50Hz	0.03 to 50Hz	$\geq DC$[a]
Temperature range	−15 °C to +55 °C	−15 °C to +55 °C	≤ 80 °C
Generator constant	$50\frac{\text{Vs}}{\text{rad}}$	$50\frac{\text{Vs}}{\text{rad}}$	$5 \cdot 10^6 \frac{\text{counts}}{\text{rad/s}}$
Self noise level	≤ 1 μrad/s RMS	0.5 μrad/s RMS	0.2 μrad/s at 0.1Hz[b]
Power consumption	0.2W at 12V	0.5W at 12V	25W at 24V

([a] The upper frequency limit determined by sensor electronics is at 386 kHz. At very low frequencies ($\ll 0.01$ Hz), the sensor drift caused by random walk makes the readout unreliable (personal communication with the manufacturer). Testing the instrument at such low frequencies was not subject of this work. [b] This value was measured by the authors of this article)

thus effective acceleration of the fluid a lead to a current of ions through the transducer depending on dynamic viscosity and thereby on the fluid temperature. When testing the temperature dependency of the generator constant, it should thus be possible to see increasing output voltage with higher temperatures. The R1 and R2 signals were digitized by a RefTek RT130 data acquisition unit with a σ/δ AD-converter at a sampling rate of 200 sps.

The LCG-Demonstrator is based on the LCR-100 AHRS in serial production since 2007 by Northrop Grumman LITEF. This device serves as a first demonstrator version for a specific new product adapted to seismology and civil engineering. The LCG-Demonstrator (Fig. 2) works in principle as a fiber optic gyroscope (Schreiber et al. 2009b). The phase difference $\Delta\varphi$ between two counter propagating light beams depends on the number of turns of fiber N, the enclosed area A, the speed of light c_0, the wave length λ, and the angular velocity $\hat{\Omega}$ with which the whole arrangement is rotating:

$$\Delta\varphi = \frac{8\pi N\mathbf{A}\hat{\Omega}}{c_0\lambda}. \quad (1)$$

For further details on the Sagnac effect, the reader is referred to Igel et al. (2005) and Schreiber et al. (2009a). Since digitization is part of the internal signal processing, the output of the LCG-Demonstrator is a continous data stream in miniSEED format (see www.iris.edu/manuals/SEEDManual_v2.4.pdf) containing the data sampled at 200 sps which at the present stage of development can be accessed via an UDP ethernet protocol at the demonstrator and might be changed

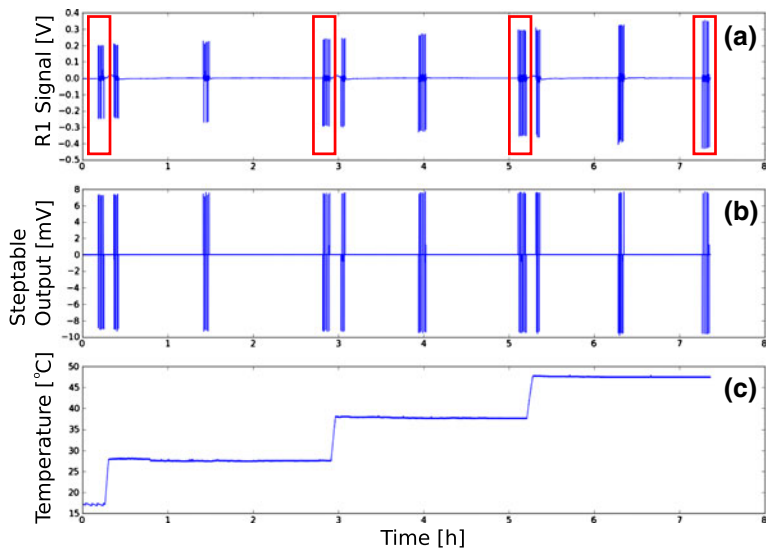

Fig. 3 The R1 signal increases **a** while the calibration signal stays constant **b** with increasing temperature **c**. The data used for analysis is marked in *red*

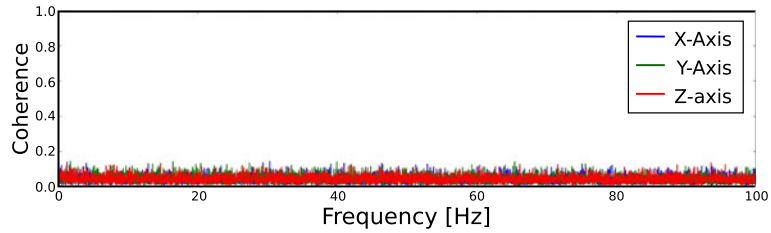

Fig. 4 The coherence spectra for all three rotational components of the LCG-Demonstrator (S/N 2056 and 2276) show that the contribution of coherent ambient noise sources was very small during the self-noise measurements

to TCP/IP for serial devices in the near future. Because of the fixed sampling rate of 200 sps, this instrument is not applicable to strong motion seismology where especially higher frequencies are of interest. For future developments, this limitation needs to be removed.

The technical data provided by the manufacturers is summarized in Table 1.

3 Measurements and data processing

All tests were carried out on an auxiliary monument of the seismic station at the Geophysical Observatory in Fürstenfeldbruck, Germany. The tests were analyzed with the software toolbox ObsPy (Beyreuther et al. 2010; Megies et al. 2011). For the absolute calibration as a function of temperature, the instruments were placed onto the tilt bridge of the calibration table Lennartz CT-EW01 (manual available at www.lennartz-electronic.de) used for absolute calibration of traditional translational motion seismometers. It produces an input step signal which has its main frequency content in the range of 1 Hz. The actual step size can be determined via two dial gauges. The constant step size of 1.013 mm and the bridge length of 400 mm give a constant input rotation angle of 0.0025 rad. Together with two simple 100-W light bulbs, the complete device was covered by an insulating styrofoam box. The bulbs were connected to a regulating circuit, and temperature could be kept constant for 2 h at approximately 20 °C, 30 °C, 40 °C, and 50 °C (±1 °C) (Fig. 3c). The signals taken for calibration (marked red in Fig. 3a) were integrated to obtain values in a unit comparable to the constant input rotation angle (Fig. 3b). The corresponding output step sizes were divided by this rotation angle, and the final result is the average over 15 to 20 steps.

Estimating the incoherent self-noise of an instrument is equivalent to measure the output of the instrument without any contribution of input ground movement or other ambient noise sources. In order to perform the self-noise tests, we placed the R1, the R2, and two of the LCG-Demonstrators onto an approximately 3-cm-thick

Table 2 Self-noise types and the corresponding exponents of the power laws $\bar{Y}(f) \propto f^{\alpha}$ and $\sigma_y^2(\tau) \propto \tau^{\mu}$ (see Barnes 1970)

Process type	α	μ
White noise (phase modulated)	+2	n.d.
Flicker noise (phase modulated)	+1	−2
White noise (amplitude modulated)	0	−1
Flicker noise (amplitude modulated)	−1	0
Random walk (amplitude modulated)	−2	+1

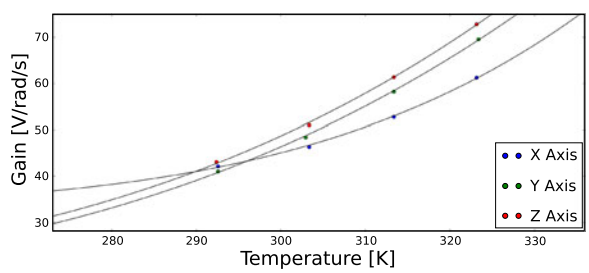

Fig. 5 In a temperature range from 20 °C to 50 °C, the generator constant of the R1 deviates up to 27% from the nominal value of 50 V/rad/s. The *black lines* represent a fitted Arrhenius function

Table 3 The generator constant, G, of the R2 deviates up to 18% from the nominal value of 50 V/rad/s in a temperature range from 20 °C to 50 °C

X		Y		Z	
T (°C)	G (V/rad/s)	T (°C)	G (V/rad/s)	T (°C)	G (V/rad/s)
19.6	37.5 ± 0.3	19.6	38.9 ± 0.6	19.2	27.1 ± 0.5
30.3	34.0 ± 0.6	30.6	34.3 ± 0.6	30.5	27.1 ± 0.3
41.2	32.2 ± 0.7	41.4	30.9 ± 0.6	41.0	26.1 ± 0.4
51.9	29.9 ± 0.8	51.6	27.6 ± 0.4	51.6	22.9 ± 0.4

Smaller values for higher temperatures indicate overcompensation of temperature deviations

slab of gabro which could be leveled with three pin-shaped screw feet. We are confident that this setup guaranteed that scattering or bending effects of the monument or plate which would produce incoherent noise were negligible. Therefore the assumption that sensor self-noise is the only incoherent noise source is justified. The small values of coherence in the coherence spectra for the three rotational channels of the LCG-Demonstrator (Fig. 4) prove that the contribution of coherent ambient noise sources was very small.

Nevertheless, the tests were analyzed using the three-channel correlation method introduced by Sleeman (2006), which provides the possibility to further minimize the contribution of coherent noise sources in the results. Assuming that three collocated instruments feel the same ambient noise signals, it is possible to estimate the power spectral density (PSD) of the self-noise N_{ii} of the sensor i using:

$$N_{ii} = \bar{Y}_{ii} - \bar{Y}_{ji} \cdot \frac{\bar{Y}_{ik}}{\bar{Y}_{jk}}. \tag{2}$$

$\bar{Y}_{ii}$ and $\bar{Y}_{ji}$ are the power- and cross-power spectral densities of the sensors i and j. The PSDs were estimated with Welch's modified periodogram method (Welch 1967). Time segments of 200 s were modified with a Hann window function and overlapped with a fraction of 7/8. The total length of the analyzed data was 3 h. The operating range diagram representation (see Evans et al. 2010) is used to compare the self-noise levels with the maximum amplitude of the Tohoku earthquake ($M_W = 9.0$), March 11 2011, recorded by the ring laser gyroscope G in Wettzell.

An additional characterization of the self-noise processes in the instruments was done by a method first introduced by Allan (1966). Averaging the self-noise time series y_k over a certain time bin τ, taking the two-sample variance of these averages for successive, non-overlapping time bins, and averaging this variances over the total time series give the Allan variance $\sigma_y^2(\tau)$ (see Barnes 1970):

$$\sigma_y^2(\tau) = \left\langle \frac{(\bar{y}_{k+1} - \bar{y}_k)^2}{2} \right\rangle. \tag{3}$$

$\bar{y}_k$ is the k-th average value of the signal y over the time bin τ and $\langle\rangle$ denotes the infinite time average. If the PSD of a noise process in a certain frequency range follows a power law $\bar{Y}(f) \propto f^{\alpha}$, then the Allan variance $\sigma_y^2(\tau)$ follows a similar power law $\sigma_y^2(\tau) \propto \tau^{\mu}$ with $\mu = -\alpha - 1$ and $-3 \leq \alpha \leq 1$. Plotting $\sigma_y^2(\tau)$ on a logarithmic scale over the averaging time τ, the slope of the graph is directly related to the type of the dominating noise process in the observed frequency range

Table 4 The temperature compensation in the closed-loop system LCG-Demonstrator works very well

X		Y		Z	
T (°C)	G (10^6/rad/s)	T (°C)	G (10^6/rad/s)	T (°C)	G (10^6/rad/s)
20.3	4.95 ± 0.07	20.4	4.95 ± 0.09	20.5	4.97 ± 0.08
31.7	4.98 ± 0.08	31.3	4.96 ± 0.08	31.8	4.98 ± 0.08
41.9	4.98 ± 0.08	41.6	4.95 ± 0.09	42.0	4.96 ± 0.08
51.8	4.97 ± 0.07	52.2	4.96 ± 0.08	52.2	4.96 ± 0.08

The generator constant, G, can be seen as constant within the error bars

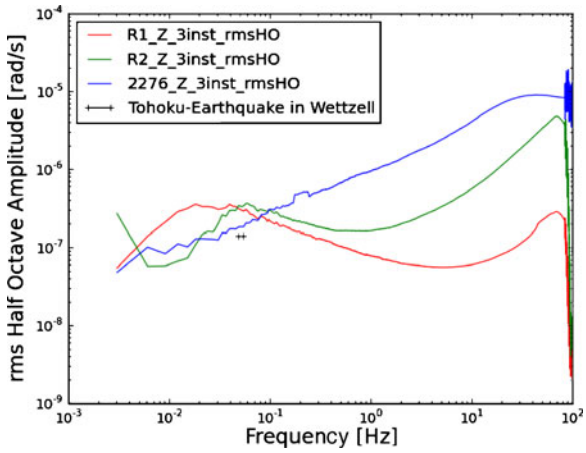

Fig. 6 The operating range diagrams for the LCG-Demonstrator (S/N 2276), the R1, and the R2 (Z-axis) show that the instruments would not have recorded the Tohoku earthquake in Wettzell

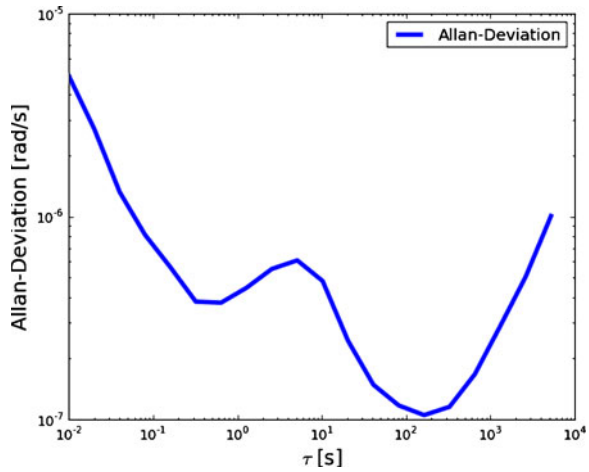

Fig. 8 Allan deviation of the R2 (Z-axis); the local peak within 0.6 and 50 s may be related to non-linear transfer function of the instrument in that period range

(see Barnes 1970). Table 2 summarizes the relationship between the exponents α and μ and the corresponding noise processes. The Allan deviation is defined by the square root of the Allan variance.

4 Results

As a very prominent result the estimated temperature dependency of the R1 (and R2) is surprisingly large. In a temperature range from 20 °C to 50 °C, the generator constant of the R1 deviates up to 27% from the nominal value of 50 V/rad/s (Fig. 5). Following physics textbooks, the dependence of dynamic viscosity η on temperature is described by an Arrhenius law:

$$\eta(T) = \eta_0 e^{C/T}, \tag{4}$$

where η_0 and C are material-specific constants. The black lines in Fig. 5 represent a fitted

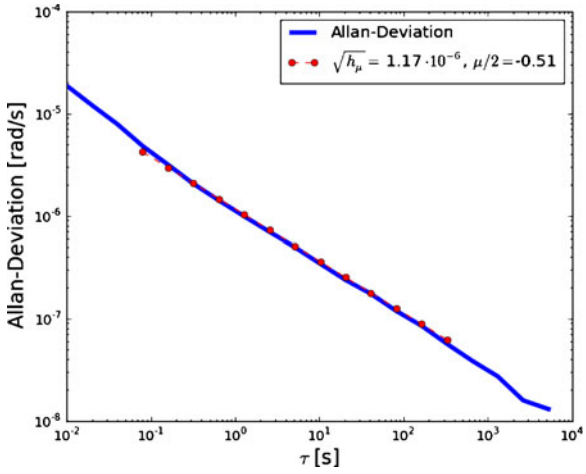

Fig. 7 The Allan deviation of the LCG-Demonstrator (S/N 2276, Z-axis) indicates amplitude-modulated white noise ($\mu = -1$) for periods from 0.1 to 500 s

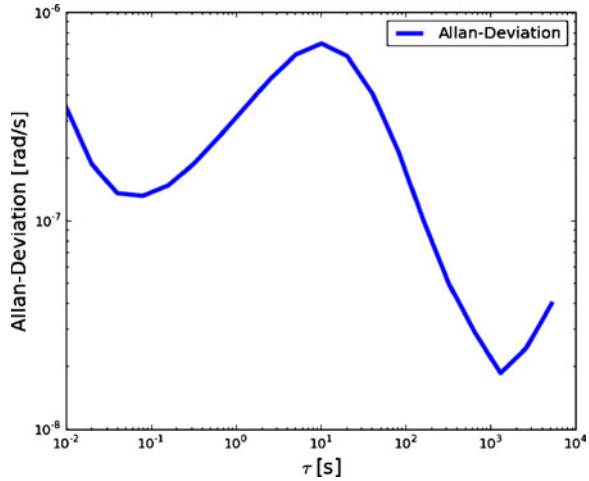

Fig. 9 Allan deviation of the R1 (Z-axis); similar to the R2 sensor the form of the Allan variance in the period range from 0.1 to 1,000 s might be related to non-linearity of the transfer function of the instrument in this period range

Arrhenius function and show that the temperature dependence of the generator constant of the R1 can be explained solely with the variation of dynamic viscosity. The generator constant of the R2 deviates up to 18% from the nominal value of 50 V/rad/s in a temperature range from 20 °C to 50 °C (Table 3). Smaller values for higher temperatures indicate overcompensation of temperature deviations. For the LCG-Demonstrator, the generator constant can be taken as constant within the error bars (Table 4) leading to the conclusion that the compensation in the closed-loop system works very well.

The operating range diagrams for the LCG-Demonstrator (S/N 2276), the R1, and the R2 (Z-axis) reveal that for weak motion applications, the sensitivity of all tested instruments has to be improved by at least one order of magnitude or better (Fig. 6). The self-noise amplitudes in a period range from 10 to 100 s are up to one magnitude larger than the maximum amplitude of the Tohoku earthquake recorded by the ring laser gyroscope in Wettzell.

The Allan deviation of the LCG-Demonstrator indicates amplitude-modulated white noise ($\mu = -1$) for periods from 0.1 to 500 s (Fig. 7). The local peak within 0.6 and 50 s, which can be seen in the Allan deviation of the R2 (Fig. 8), might be related to a somehow nonlinear transfer function and reflects the fluid-based sensor design in that period range. The same is true for the R1. Here abnormal behavior occurs in a period range from 0.1 to 1,000 s which includes a significant fraction of the sensor pass band (Fig. 9). For both instruments, this behavior was constant with time.

5 Conclusion

We performed tests on the temperature stability of the generator constant and characterized the instrument self-noise of the fiber optic gyro-based LCG-Demonstrator and the liquid-based rotational seismometers R1 and R2. Observing a deviation of 27% and 18% of the generator constants of the R1 and R2 from the nominal value in a temperature range from 20 °C to 50 °C, we conclude that the liquid-based technology has to be further improved for reliable field measurements. In the same temperature range, the generator constant of the LCG-Demonstrator can be seen as constant and with an average of 4.97×10^6 rad/s^{-1}, it meets the nominal value. The self-noise amplitudes in the order of 10^{-7} rad/s in the period range of 10 to 100 s are seen as to be too high for seismic weak motion applications. The 25 W-power consumption and the rather low sensitivity of the LCG-Demonstrator contradict our a-priori general requirements for rotational motion sensors and do not permit field installation or weak motion seismology. Its present version, however, might be very useful in civil engineering applications, when constant power supply is at hand and strong signals are the main focus of interest (monitoring buildings in earthquake regions and online monitoring of wind power plants). In this context, further field tests are needed to fully exploit the benefit of rotational motion sensors in seismological applications.

Acknowledgements We would like to thank the editor of this special issue, J. R. Evans, and our two reviewers whose comments were very helpful. We would also like to thank the team of Northrop Grumman LITEF for their efficient cooperation and C. Sens-Schoenfelder for making the R2 available. This work was partially funded by the Deutsche Forschungsgemeinschaft in the project number Ig16/8.

References

Allan DW (1966) Statistics of atomic frequency standards. Proc IEEE 54:221–230

Barnes JA (1970) Characterization of frequency stability. National Bureau of Standards Technical Note 394. http://tf.boulder.nist.gov/general/pdf/264.pdf

Beyreuther M, Barsch R, Krischer L, Megies T, Behr Y, Wassermann J (2010) Obspy: a python toolbox for seismology. Seismol Res Lett 81:530–533. doi:10.1785/gssrl.81.3.530

Cochard A, Igel H, Schuberth B, Suryanto W, Velikoseltsev A, Schreiber U, Wassermann J, Scherbaum F, Vollmer D (2006) Rotational motions in seismology: theory, observation, simulation. Springer, New York, pp 391–411

Eentec (2006) Electrochemical sensor transducers. http://www.eentec.com/pdf/ELECTROCHEMICA-1.pdf

Evans JR, Followill F, Hutt CR, Kromer RP, Nigbor RL, Ringler AT, Steim JM, Wielandt E (2010) Method for calculating self-noise spectra and operating ranges for seismographic inertial sensors and recorders. Seismol Res Lett 81(4):640–646. doi:10.1785/gssrl.81.4.640

Graizer V (2006) Tilts in strong ground motion. Bull Seismol Soc Am 96(6):2090–2102. doi:10.1785/0120060065

Graizer V (2010) Strong motion recordings and residual displacements: what are we actually recording in strong motion seismology? Seismol Res Lett 81(4): 635–639. doi:10.1785/gssrl.81.4.635

Igel H, Schreiber U, Flaws A, Schuberth B, Velikoseltsev A, Cochard A (2005) Rotational motions induced by the M8.1 Tokachi-Oki earthquake. Geophys Res Lett 32:1–5. doi:10.1029/2004GL022336

Lin CJ, Liu CC, Lee WHK (2009) Recording rotational and translational ground motions of two TAIGER explosions in northeastern Taiwan on 4 March 2008. Bull Seismol Soc Am 99(2B):1237–1250. doi:10.1785/0120080176

Megies T, Beyreuther M, Barsch R, Krischer L, Wassermann J (2011) Obspy what can it do for data centers and observatories? Ann Geophys 54(1):47–58

Nigbor RL, Evans JR, Hutt CR (2009) Laboratory and field testing of commercial rotational seismometers. Bull Seismol Soc Am 99(2):1215–1227. doi:10.1785/0120080247

Schreiber KU, Hautmann JN, Velikoseltsev A, Wassermann J, Igel H, Otero J, Vernon F, Wells JPR (2009a) Ring laser measurements of ground rotations for seismology. Bull Seismol Soc Am 99(2B): 1190–1198. doi:10.1785/0120080171

Schreiber KU, Velikoseltsev A, Carr AJ, Franco-Anaya R (2009b) The application of fiber optic gyroscopes for the measurement of rotations in structural engineering. Bull Seismol Soc Am 99(2B):1207–1214. doi:10.1785/0120080086

Sleeman R (2006) Three-channel correlation analysis: a new technique to measure instrumental noise of digitizers and seismic sensors. Bull Seismol Soc Am 96(1):258–271. doi:10.1785/0120050032

Welch PD (1967) The use of fast fourier transform for the estimation of power spectra: a method based on time averaging over short, modified periodograms. IEEE Trans Audio Electroacoust AU-15:70–73